

# High-harmonic generation in spin and charge current pumping at ferromagnetic or antiferromagnetic resonance in the presence of spin-orbit coupling

J. Varela Manjarres,<sup>1</sup> O. Ly,<sup>2</sup> A. Manchon,<sup>2,3</sup> T. Kloss,<sup>4</sup> X. Waintal,<sup>4</sup> and B. K. Nikolić<sup>1,\*</sup>

<sup>1</sup>*Department of Physics and Astronomy, University of Delaware, Newark, DE 19716, USA*

<sup>2</sup>*Physical Science and Engineering Division (PSE),*

*King Abdullah University of Science and Technology (KAUST), Thuwal 23955-6900, Saudi Arabia*

<sup>3</sup>*Aix-Marseille Univ, CNRS, CINaM, Marseille, France*

<sup>4</sup>*Université Grenoble Alpes, CEA, IRIG-PHELIQS, 38000 Grenoble, France*

One of the cornerstone effects in spintronics is spin pumping by dynamical magnetization that is steadily precessing (around, e.g., the  $z$ -axis) with frequency  $\omega_0$ , due to absorption of *low-power* microwaves of frequency  $\omega_0$  under the resonance conditions and in the *absence* of any applied bias voltage. The two-decades-old “standard model” of this effect, based on the scattering approach of quantum transport attuned to the problem of adiabatic pumping of spin or charge, predicts that component  $I^{S_z}$  of spin current vector  $(I^{S_x}, I^{S_y}, I^{S_z}) \propto \omega_0$  is *time-independent* while  $I^{S_x}(t)$  and  $I^{S_y}(t)$  oscillate harmonically in time with *single* frequency  $\omega_0$ ; whereas pumped charge current is zero  $I \equiv 0$  in the same adiabatic  $\propto \omega_0$  limit. Here we employ more general time-dependent quantum transport formalism to predict unforeseen features of spin pumping—precessing localized magnetic moments within ferromagnetic metal (FM) or antiferromagnetic metal (AFM), whose conduction electrons are exposed to spin-orbit (SO) coupling of either intrinsic or proximity origin, will pump *both* spin  $I^{S_\alpha}(t)$  and charge  $I(t)$  currents. All four of these functions harmonically oscillate in time at both *even and odd* integer multiples  $n\omega_0$  of the driving frequency  $\omega_0$ . Such high harmonics are cut off at  $n_{\max}$ , with possibility to tune  $n_{\max} \leq 4$  in our chosen one-dimensional FM or AFM models by increasing the strength of their Rashba SO coupling.

**Introduction.**—The pumping of electronic spin current by dynamical magnetization of a ferromagnetic metal (FM) layer into adjacent normal metal (NM) layer was discovered [1] originally for steadily precessing magnetization of FM due to the absorption of *low-power* ( $\sim$  mW [2]) microwaves in  $\sim$  GHz range under the ferromagnetic (F) resonance conditions. Since it occurs in the absence of any bias voltage, it is termed “pumping” akin to low-temperature quantum transport where time-dependent quantum systems emit currents [3–5]. This has turned out to be a ubiquitous phenomenon in room-temperature spintronic devices, emerging whenever dynamics of localized magnetic moments is initiated—such as by external electromagnetic radiation or static magnetic fields—and dynamical magnetic moments interact with conduction electrons to drive them out of equilibrium. For example, recent observations include spin pumping into adjacent NM from microwave-driven ferromagnetic and ferri-magnetic insulators [6], antiferromagnetic (AF) insulators [7, 8], as well as from any dynamical non-collinear magnetic texture (such as domain walls [9–12], skyrmions [13] and spin waves [14]).

Despite being quintessentially a quantum transport phenomenon, spin pumping is observed even at room temperature because of its interfacial nature [1] where the relevant region around magnetic-material/NM interface is always thinner [15] than decoherence lengths for electronic orbital and spin degrees of freedom. Thus, the “standard model” [1] of spin pumping is built using the scattering theory [4] of quantum transport to describe how magnetization of ferromagnets, or both the Néel vector and nonequilibrium magnetization of antiferromag-

nets [7, 8, 16], precessing with frequency  $\omega_0$  around the easy ( $z$ -axis) pushes electrons out of equilibrium. The ensuing flowing electronic spins comprise spin current vector  $(I^{S_x}(t), I^{S_y}(t), I^{S_z})$  whose  $I^{S_z}$  component is *time-independent* while  $I^{S_x}(t)$  and  $I^{S_y}(t)$  oscillate harmonically in time at a *single* frequency  $\omega_0$  [1]. These DC and AC components of pumped spin current can be converted into DC [17] and AC [18] voltages, respectively, by the inverse spin Hall effect and then measured using standard electrical circuits. The magnitude of each component is  $\propto \omega_0$ , as the signature of general adiabatic quantum pumping [3–5], as well as  $\propto \sin^2 \theta$  [1, 15] where the precession cone angle  $\theta$  is controlled by the input microwave power [2, 19]. The spin pumping generates effectively additional dissipation [1, 9, 12] for the magnetization dynamics, so that such loss of spin angular momentum can be employed for indirect [1, 10] detection of pumping.

Thus, the “standard model” of spin pumping *excludes* possibility of time-dependent  $I^{S_z}(t)$  or higher harmonics in periodic time dependence of any of the three components of pumped spin current. Alternatives to “standard model” include Floquet nonequilibrium Green’s function (NEGF) [20–22] or the Kubo formalism [24], developed in order to include possibly strong spin-orbit (SO) coupling directly at the F(AF)-material/NM interface where the analytical formula of the “standard model” ceases to be applicable [1, 20, 21, 23]. However, these alternatives are designed to compute time-averaged value of pumped spin or charge currents, so any high harmonic in periodic time dependence of  $I^{S_\alpha}(t)$  ( $\alpha \in \{x, y, z\}$ ) or  $I(t)$  is overlooked by them as well. Extending [25, 26] Floquet-NEGF formalism to obtain complete periodic time dependence,

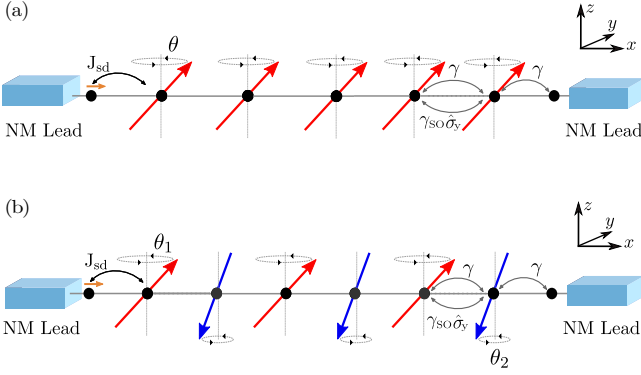


FIG. 1. Schematic view of two-terminal setups modeled on 1D TB lattice where magnetic moments within (a) FM or (b) AFM in the central region, attached to two semi-infinite NM leads, are steadily precessing with frequency  $\omega_0$  around the  $z$ -axis due to resonant absorption of  $\sim$  GHz or  $\sim$  THz microwaves, respectively. The precession cone angle is  $\theta$  in the FM case; or  $\theta_1 > \theta_2$  for two sublattices in the RH mode of precession [7, 16] in the AFM case. In the absence of any bias voltage between macroscopic reservoirs into which NM leads terminate, dynamical magnetic moments interact with electrons via  $sd$  exchange coupling  $J_{sd}$  to drive them out of equilibrium and pump time-dependent spin  $I^{S\alpha}(t)$  and charge  $I(t)$  currents into the NM leads. Electrons hop between the sites with parameter  $\gamma$ , as well as with an additional [Eq. (1)] spin-dependent hopping  $\gamma_{SO}$  [32] describing the Rashba SO coupling [30] within the central region.

$I^{S\alpha}(t) = I^{S\alpha}(t + 2\pi/\omega_0)$  and  $I(t) = I(t + 2\pi/\omega_0)$ , would detect integer high harmonics, but it would miss any possibility of non-integer [27] harmonics (or interharmonics, as they are called in engineering literature [28]).

In this Letter, we apply to two-terminal setups illustrated in Fig. 1 time-dependent NEGF (TDNEGF) formalism [29] approach to quantum transport, which is more general than prior scattering [1, 16] or Floquet-NEGF [20–22] theories of spin pumping, and can yield both transient and (at longer times) time-periodic pumped spin and charge currents in *numerically exact* fashion. In Fig. 1(a) FM, and in Fig. 1(b) antiferromagnetic metal (AFM), host both magnetic moments and conduction electrons subject to the Rashba type of SO coupling [30] throughout the whole magnetic region. These FM or AFM regions are sandwiched between two semi-infinite NM leads terminating into macroscopic reservoirs kept at the same chemical potential  $\mu_L = \mu_R = 0$  (so, lattices in Fig. 1 are half filled by electrons) and temperature  $T = 300$  K [31]. Starting from equilibrium state described by grand canonical density matrix [see Eq. (4) in Ref. [11]], all magnetic moments modeled as classical vectors  $\mathbf{M}_i$  of unit length start to precess uniformly at time  $t = 0$  around the  $z$ -axis with frequency  $\omega_0$  and precession cone angle  $\theta$  in the case of FM; or with precession cone angles  $\theta_1$  and  $\theta_2$  for magnetic moments  $\mathbf{M}_i$  on sublattice  $A$  and  $\mathbf{M}_{i+1}$  on sublattice  $B$

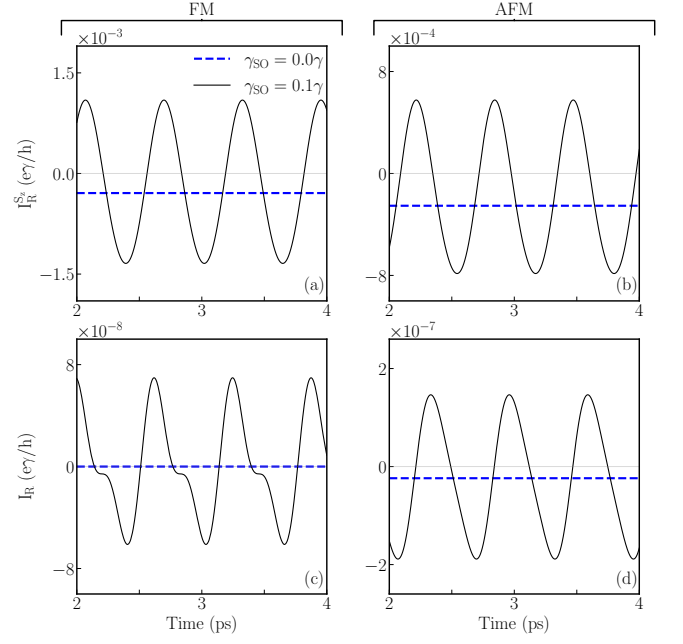


FIG. 2. Time-dependence of (a), (b) spin  $I_R^{S_z}(t)$  and (c), (d) charge  $I_R(t)$  currents, after the transient response has died out, pumped into the right NM lead in (a), (c) FM setup or (b), (d) AFM setup. The Rashba SO coupling [Eq. (1)] is turned off ( $\gamma_{SO} = 0$ ) or turned on ( $\gamma_{SO} = 0.1\gamma = J_{sd}$ ) within the entire magnetic region in Fig. 1.

of AFM. Our principal results in Figs. 2–4 for pumping at F or AF resonance show that, once the Rashba SO coupling is turned on,  $I^{S_z}(t)$  becomes time-dependent [Figs. 2(a) and 2(b)] and pumping of nonzero charge current  $I(t)$  [Figs. 2(c) and 2(d)] ensues as well. Both of these types of current contain high harmonics [Figs. 3] in their periodic time dependence at *both* even and odd integer multiples  $n\omega_0$  of the driving frequency  $\omega_0$  whose cutoff  $n_{\max}$  can be controlled by the strength of the SO coupling [Fig. 4]. Prior to delving into these results, we introduce useful concepts and notation.

*Models and methods.*—The electronic system within FM [Fig. 1(a)] or AFM [Fig. 1(b)] region is modeled by a one-dimensional (1D) tight-binding (TB) Hamiltonian

$$\hat{H}(t) = -\gamma \sum_{\langle ij \rangle} \hat{c}_i^\dagger \hat{c}_j - \gamma_{SO} \sum_{\langle ij \rangle} \hat{c}_i^\dagger \hat{\sigma}_y \hat{c}_j - J_{sd} \sum_i \hat{c}_i^\dagger \boldsymbol{\sigma} \cdot \mathbf{M}_i(t) \hat{c}_i, \quad (1)$$

where  $\hat{c}_i^\dagger = (\hat{c}_{i\uparrow}^\dagger, \hat{c}_{i\downarrow}^\dagger)$  is a row vector containing operators  $\hat{c}_{i\sigma}^\dagger$  which create an electron with spin  $\sigma = \uparrow, \downarrow$  at site  $i$ ;  $\hat{c}_i$  is a column vector containing the corresponding annihilation operators;  $\gamma = 1$  eV is the hopping parameter between the nearest-neighbor (signified by  $\langle \dots \rangle$ ) sites;  $\gamma_{SO}$  is an additional spin-dependent hopping [32] due to the Rashba SO coupling [30]; and the conduction electron spin, described by the vector of the Pauli matri-

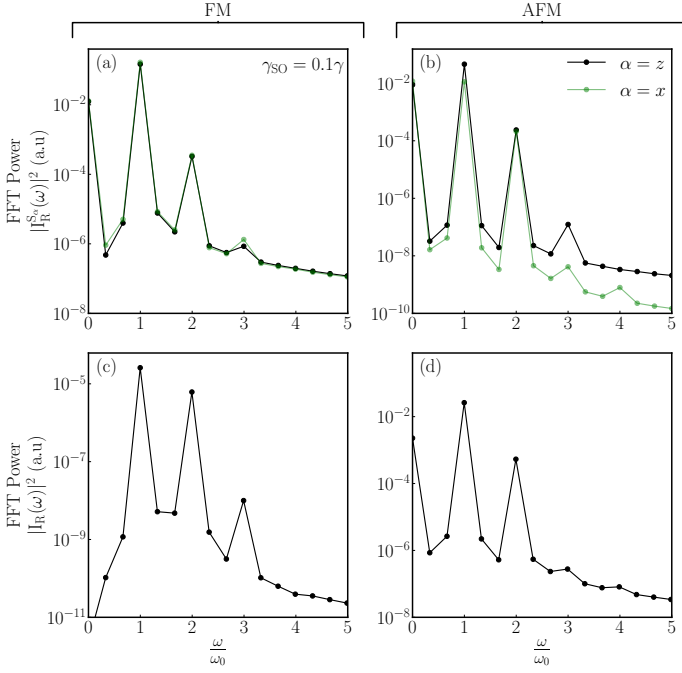


FIG. 3. High harmonics in FFT power spectrum of pumped spin  $|I_R^{S_z}(\omega)|^2$  and charge currents  $|I_R(\omega)|^2$  in Figs. 2(a)–(d), respectively. Panels (a) and (b) also show high harmonics in FFT power spectrum of pumped spin current  $|I_R^{S_x}(\omega)|^2$ .

ces  $\sigma = (\hat{\sigma}_x, \hat{\sigma}_y, \hat{\sigma}_z)$ , interacts with the classical magnetic moments  $\mathbf{M}_i(t)$  via  $sd$  exchange interaction of strength  $J_{sd} = 0.1$  eV [33]. We use  $N = 9$  ( $N = 10$ ) sites in FM (AFM) central region, which ensure maximum outflowing spin current (which in 1D oscillates as a function of  $N$  [11]). The left ( $L$ ) and the right ( $R$ ) NM leads, sandwiching FM or AFM region in Fig. 1, are semi-infinite 1D TB chains described by the first term alone in Eq. (1).

In the case of FM central region [Fig. 1(a)], all magnetic moments precess uniformly with the same frequency  $\omega_0$  and the cone angle  $\theta = 20^\circ$  (which is near the maximum that can be achieved in practice without introducing nonlinearities [2, 19]). This means that  $\mathbf{M}_i(t) = (\sin \theta \cos(\omega_0 t), \sin \theta \sin(\omega_0 t), \cos \theta)$  is plugged into Eq. (1). Let us recall that at AF resonance two precession modes of sublattice magnetic moments are possible, with left-handed (LH) and right-handed (RH) chiralities [16], where both  $\mathbf{M}_i^A(t)$  and  $\mathbf{M}_i^B(t)$  undergo a clockwise or counterclockwise precession with  $\pi$  phase difference, respectively. In the case of AFM central region [Fig. 1(b)], we use the RH mode— $\mathbf{M}_i(t) = (\sin \theta \cos(\omega_0 t), \sin \theta \sin(\omega_0 t), \cos \theta)$  and  $\mathbf{M}_{i+1}(t) = (\sin \theta \cos(\omega_0 t + \pi), \sin \theta \sin(\omega_0 t + \pi), \cos \theta)$ —where  $\theta_1 = 20^\circ$  and we fix the ratio  $\theta_1/\theta_2 = 1.29$  to correspond to the case of the RH mode of  $\text{MnF}_2$  employed in recent experiments [7]. Note that we use the same driving frequency  $\hbar\omega_0 = 0.01$  eV for both FM and AFM cases, which is realistic for the latter but too large for

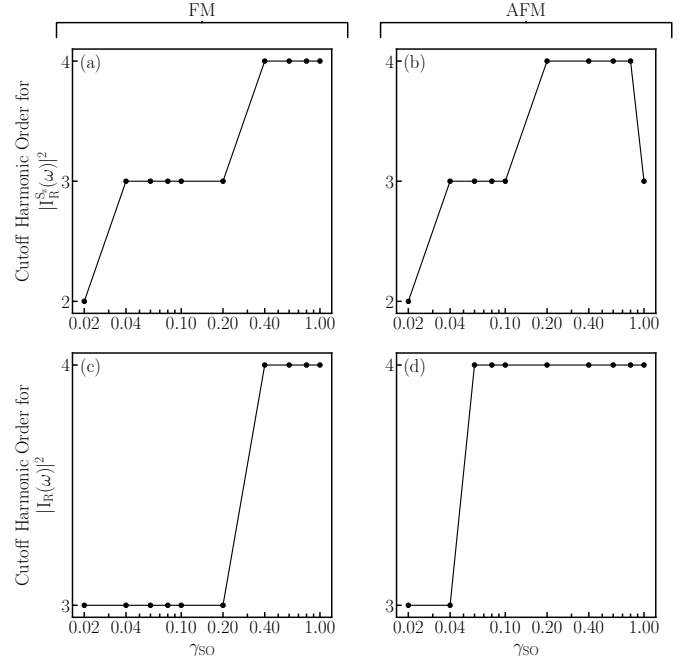


FIG. 4. (a)–(d) Cutoff harmonic order  $n_{\max} = \omega_{\max}/\omega_0$  in FFT power spectrum of pumped spin  $|I_R^{S_z}(\omega)|^2$  and charge currents  $|I_R(\omega)|^2$  in Figs. 3(a)–(d), respectively.

the former. This reduces computational expense of TD-NEGF calculations, while not affecting the result since the magnitude of all pumped currents scale linearly with  $\omega_0$  (in other words, the results for the FM case can be easily rescaled to realistic frequencies).

The fundamental quantity of quantum statistical mechanics is the density matrix. The time-dependent one-particle nonequilibrium density matrix can be expressed [29],  $\rho_{\text{neq}}(t) = \hbar \mathbf{G}^<(t, t)/i$ , in terms of the lesser Green's function of TDNEGF formalism defined by  $G_{ii'}^{<, \sigma \sigma'}(t, t') = \frac{i}{\hbar} \langle \hat{c}_{i' \sigma'}^\dagger(t') \hat{c}_{i \sigma}(t) \rangle_{\text{nes}}$  where  $\langle \dots \rangle_{\text{nes}}$  is the nonequilibrium statistical average [34]. We solve a matrix integro-differential equation [11, 31]

$$i\hbar \frac{d\rho_{\text{neq}}}{dt} = [\mathbf{H}(t), \rho_{\text{neq}}] + i \sum_{p=L,R} [\mathbf{\Pi}_p(t) + \mathbf{\Pi}_p^\dagger(t)], \quad (2)$$

for the time evolution of  $\rho_{\text{neq}}(t)$ , where  $\mathbf{H}(t)$  is the matrix representation of Hamiltonian in Eq. (1). Equation (2) is an *exact* quantum master equation for the reduced density matrix of the central FM or AFM region viewed as an open finite-size quantum system attached to macroscopic Fermi liquid reservoirs via semi-infinite NM leads. The  $\mathbf{\Pi}_p(t)$  matrices

$$\mathbf{\Pi}_p(t) = \int_{t_0}^t dt_2 [\mathbf{G}^>(t, t_2) \mathbf{\Sigma}_p^<(t_2, t) - \mathbf{G}^<(t, t_2) \mathbf{\Sigma}_p^>(t_2, t)], \quad (3)$$

are expressed in terms of the lesser and greater Green's functions [34] and the corresponding self-energies

$\Sigma_p^{><}(t, t')$  [31]. They yield directly time-dependent charge current,  $I_p(t) = \frac{e}{\hbar} \text{Tr}[\Pi_p(t)]$ , and spin current,  $I_p^{S\alpha}(t) = \frac{e}{\hbar} \text{Tr}[\hat{\sigma}_\alpha \Pi_p(t)]$ , pumped into the lead  $p = L, R$ . We use the same units for charge and spin currents, defined as  $I_p = I_p^\uparrow + I_p^\downarrow$  and  $I_p^{S\alpha} = I_p^\uparrow - I_p^\downarrow$ , in terms of spin-resolved charge currents  $I_p^\sigma$ . In our convention, *positive* current in NM lead  $p$  means charge or spin is flowing *out* of that lead. All results are independently confirmed using TDNEGF implementation within TK-WANT package [35]. Although we use 1D TB chain to model FM and AFM setups in Fig. 1, these setups can be easily converted into three-dimensional (3D) realistic junctions with macroscopic cross section by assuming that chain is disorder-free and periodically repeated in the  $y$ - and  $z$ -directions. This means that our TDNEGF calculations would have to be repeated at each  $(k_y, k_z)$  point [15]. Nevertheless, studying simpler 1D models is sufficient [15] to capture essential features of pumping from realistic 3D systems [e.g., compare Fig. 3 for 3D junction with realistic atomistic structure to Fig. 4 for 1D junction in Ref. [22]].

*Results and discussion.*—We warm up with calculations [flat dashed lines in Fig. 2] reproducing “standard model” results for spin pumping from FM [1] or AFM [16] in the absence of SO coupling,  $\gamma_{\text{SO}} = 0$ . As expected, our TDNEGF calculations reproduce time-independent  $I_p^{S_z}$  and  $I_p = 0$  (in the FM case) at sufficiently long times, after the transient response has died out. However, as soon as the Rashba SO coupling is turned on,  $I_p^{S_z}(t)$  oscillates harmonically in the long time limit and a nonzero time-periodic  $I(t)$  is established in the same limit. Note that DC currents for  $\gamma_{\text{SO}} = 0$  or perfectly harmonic currents for  $\gamma_{\text{SO}} \neq 0$  in the long time limit are ensured by continuous energy spectrum of setups in Fig. 1 brought by attached NM leads and, thereby, dissipation effects generated by fermionic reservoirs.

The emergence of  $I_p^{S_z}(t)$  and  $I(t)$  can be understood from the rotating frame picture of spin pumping [15, 36–38] where time-dependent setups in Fig. 1, with SO coupling switched off, are mapped onto four-terminal time-independent ones by unitary transformation into the frame which rotates with magnetization. Thus, in the rotating frame  $I_p^{S_z}$  is time-independent, and it remains so upon transforming it into the lab frame, while  $I = 0$  in symmetric FM devices. However, SO coupling turned on becomes time-dependent in the rotating frame, thereby pumping additional currents  $I_p^{S_z}(t)$  and  $I(t)$  on the top of those driven by effective bias voltage  $\hbar\omega_0$  [15, 37] between the left or right pairs of leads in that frame.

The *general requirements* [5, 39, 40] for the appearance of nonzero DC component (i.e., integral over one time period [20]) of pumped charge current—the left-right symmetry of a two-terminal device must be *broken*—help to validate correctness of TDNEGF calculations. If this is done by breaking both inversion symmetry and time-reversal symmetry dynamically (such as by two spatially

separated potentials oscillating out-of-phase [3–5]) then DC component of charge current is nonzero and  $\propto \omega_0$  at (sufficiently low) driving frequencies. If only one of those two symmetries is broken, and this does not have to occur dynamically, then the DC component of pumped current is  $\propto \omega_0^2$  as the signature of *nonadiabatic* charge pumping [5, 15, 39, 40]. Since FM setup in Fig. 1(a) is left-right symmetric, DC component of pumped charge current in the presence of SO coupling is zero in Fig. 2(c). Conversely, AFM setup in Fig. 1(b) has broken (by configuration of magnetic moments) left-right symmetry, so the DC component of its pumped charge current is nonzero in Fig. 2(d) for both zero and nonzero SO coupling.

Figure 3 shows that upon turning the Rashba SO coupling on, fast Fourier transform (FFT) power spectrum of pumped spin (note that spectra of  $|I_z^S(\omega)|^2$  and  $|I_x^S(\omega)|^2$  are nearly identical) and charge currents contain high-harmonics at frequencies  $n = \omega/\omega_0$  for *both* even and odd integer  $n$ . The cutoff harmonic order  $n_{\text{max}}$  can be increased [41], but only slightly [Fig. 4], by increasing the SO coupling. We anticipate that harmonics higher than  $n_{\text{max}} = 4$  [Fig. 4], or perhaps even non-integer harmonics, could be possible for more complex materials and their SO-split band structures [27, 42] than simplistic Rashba SO coupling in 1D employed in Fig. 1 to demonstrate high-harmonic generation in spin and charge pumping from spintronic devices as a proof of principle.

*Conclusions and outlook.*—The predicted high harmonic spectra [Fig. 4] for spin and charge currents pumped by precessing magnetization bear some resemblance to a field where high-harmonic generation is intensely pursued—solids driven out of equilibrium by laser light of frequency  $\omega_0$  [43]. For example, inversion symmetric bulk semiconductors driven by strong mid-infrared laser light, whose  $\hbar\omega_0$  is much smaller than the band gap, can exhibit nonlinear effect generating new radiation at odd multiples of  $\omega_0$  [43]. Furthermore, in two-dimensional (2D) systems breaking inversion symmetry, such as monolayer of MoS<sub>2</sub> [43] or surface states of topological insulators [44], additional even-order harmonics or non-integer harmonics [44] can emerge. This has inspired recent theoretical studies on possible high harmonic generation in spin currents pumped by laser light irradiating magnetic insulators [45, 46] or SO-split 2D electron gases [42] (note that in the latter case, cut-off harmonic order increases linearly with the Rashba SO coupling strength, unlike our result in Fig. 4). However, these schemes rely on highly nonlinear effects in strong light-matter coupling, and in the case of magnetic insulators they assume coupling of magnetic field of laser light to quantum (as opposed to our classical) magnetic moments. Since such coupling is  $1/c$  smaller than light-charge coupling, they would require intense THz laser pulses beyond presently available technologies.

On the other hand, setups in Fig. 1 are routinely made in spintronics using widely available microwave



sources and, in contrast to optical pumping, with *low input power*  $\sim$  mW [2] and possibility for scalability. For example, first-principles Floquet-NEGF analysis [22] of the very recent experiments [7] on spin pumping from AF insulator  $\text{MnF}_2$  in contact with heavy metal Pt has revealed that  $\text{MnF}_2$  layer can be significantly modified by SO-proximity effect [21, 22, 47–49] within such heterostructure due to SO couplings at interfaces or from the bulk of Pt layer. This means that re-examining such experiments—where all key ingredients for our predictions are already present, such as precessing classical magnetic moments driving out of equilibrium quantum electrons subject to (proximity) SO coupling [41]—could reveal high harmonics in radiation produced by time-dependent charge pumping [Figs. 2(d) and 3(d)] or spin pumping [Figs. 2(b) and 3(b)] converted to charge current [18] by Pt layer. Alternatively, one could search for F or AF materials with strong intrinsic SO coupling. In this respect, 2D magnetic materials [50] are promising since their magnetic ordering at finite temperature crucially relies on magnetic anisotropy originating from strong SO coupling [51]. In addition, both 2D magnetic materials and ultrathin layers of conventional 3D magnets can be easily SO-proximitized by transition metal dichalcogenides [48, 49] or topological insulators [47]. Finally, using AF materials driven into resonance by  $\omega_0$  in sub-THz range [7, 8] means that  $I(t)$  they pump [Figs. 2(d) and 3(d)] would generate output THz radiation at multiples of the driving frequency  $\omega_0$ , thereby opening new avenue for THz spintronics where such output radiation is presently generated by more complex F [52] or AF heterostructures [53] driven by fs laser pulses.

J. V. M. and B. K. N. were supported by the US National Science Foundation (NSF) through the University of Delaware Materials Research Science and Engineering Center DMR-2011824.

---

\* [bnikolic@udel.edu](mailto:bnikolic@udel.edu)

- [1] Y. Tserkovnyak, A. Brataas, G. E. W. Bauer, and B. I. Halperin, Nonlocal magnetization dynamics in ferromagnetic heterostructures, *Rev. Mod. Phys.* **77**, 1375 (2005).
- [2] X. Fan, E. Himbeault, Y. S. Gui, A. Wirthmann, G. Williams, D. Xue, and C.-M. Hu, Electrical detection of large cone angle spin precession from the linear to the nonlinear regime, *J. Appl. Phys.* **108**, 046102 (2010).
- [3] M. Switkes, C. M. Marcus, K. Campman, and A. C. Gosard, An adiabatic quantum electron pump, *Science* **283**, 1905 (1999).
- [4] P. W. Brouwer, Scattering approach to parametric pumping, *Phys. Rev. B* **58**, R10135 (1998).
- [5] U. Bajpai, B. S. Popescu, P. Plecháč, B. K. Nikolić, L. E. F. Foa Torres, H. Ishizuka, and N. Nagaosa, Spatiotemporal dynamics of shift current quantum pumping by femtosecond light pulse, *J. Phys.: Mater.* **2**, 025004 (2019).
- [6] F. Yang and P. C. Hammel, FMR-driven spin pumping in  $\text{Y}_3\text{Fe}_5\text{O}_{12}$ -based structures, *J. Phys. D: Appl. Phys.* **51**, 253001 (2018).
- [7] P. Vaidya, S. A. Morley, J. van Tol, Y. Liu, R. Cheng, A. Brataas, D. Lederman, and E. del Barco, Subterahertz spin pumping from an insulating antiferromagnet, *Science* **368**, 160 (2020).
- [8] J. Li *et al.*, Spin current from sub-terahertz-generated antiferromagnetic magnons, *Nature* **578**, 70 (2020).
- [9] S. Zhang and S. S.-L. Zhang, Generalization of the Landau-Lifshitz-Gilbert equation for conducting ferromagnets, *Phys. Rev. Lett.* **102**, 086601 (2009).
- [10] T. Weindler, H. G. Bauer, R. Islinger, B. Boehm, J.-Y. Chauleau, and C. H. Back, Magnetic damping: Domain wall dynamics versus local ferromagnetic resonance, *Phys. Rev. Lett.* **113**, 237204 (2014).
- [11] M. D. Petrović, B. S. Popescu, U. Bajpai, P. Plecháč, and B. K. Nikolić, Spin and charge pumping by a steady or pulse-current-driven magnetic domain wall: A self-consistent multiscale time-dependent quantum-classical hybrid approach, *Phys. Rev. Appl.* **10**, 054038 (2018).
- [12] M. D. Petrović, U. Bajpai, P. Plecháč, and B. K. Nikolić, Annihilation of topological solitons in magnetism with spin wave burst finale: The role of nonequilibrium electrons causing nonlocal damping and spin pumping over ultrabroadband frequency range, *Phys. Rev. B* **104**, L020407 (2021).
- [13] A. Abbout, J. Weston, X. Waintal, and A. Manchon, Cooperative charge pumping and enhanced skyrmion mobility, *Phys. Rev. Lett.* **121**, 257203 (2018).
- [14] A. Suresh, U. Bajpai, and B. K. Nikolić, Magnon-driven chiral charge and spin pumping and electron-magnon scattering from time-dependent quantum transport combined with classical atomistic spin dynamics, *Phys. Rev. B* **101**, 214412 (2020).
- [15] S.-H. Chen, C.-R. Chang, J. Q. Xiao, and B. K. Nikolić, Spin and charge pumping in magnetic tunnel junctions with precessing magnetization: A nonequilibrium Green function approach, *Phys. Rev. B* **79**, 054424 (2009).
- [16] R. Cheng, J. Xiao, Q. Niu, and A. Brataas, Spin Pumping and spin-transfer torques in antiferromagnets, *Phys. Rev. Lett.* **113**, 057601 (2014).
- [17] E. Saitoh, M. Ueda, H. Miyajima, and G. Tatara, Conversion of spin current into charge current at room temperature: Inverse spin-Hall effect, *Appl. Phys. Lett.* **88**, 182509 (2006).
- [18] D. Wei, M. Obstbaum, M. Ribow, C. H. Back, and G. Woltersdorf, Spin Hall voltages from a.c. and d.c. spin currents, *Nat. Commun.* **5**, 3768 (2014).
- [19] M. Jamali, J. S. Lee, J. S. Jeong, F. Mahfouzi, Y. Lv, Z. Zhao, B. K. Nikolić, K. A. Mkhoyan, N. Samarth, and J.-P. Wang, Giant spin pumping and inverse spin Hall effect in the presence of surface and bulk spin-orbit coupling of topological insulator  $\text{Bi}_2\text{Se}_3$ , *Nano Lett.* **15**, 7126 (2015).
- [20] F. Mahfouzi, J. Fabian, N. Nagaosa, and B. K. Nikolić, Charge pumping by magnetization dynamics in magnetic and semimagnetic tunnel junctions with interfacial Rashba or bulk extrinsic spin-orbit coupling, *Phys. Rev. B* **85**, 054406 (2012).
- [21] K. Dolui, U. Bajpai, and B. K. Nikolić, Effective spin-mixing conductance of topological-insulator/ferromagnet and heavy-metal/ferromagnet spin-orbit-coupled interfaces: A first-principles Floquet-nonequilibrium Green

- function approach, *Phys. Rev. Mater.* **4**, 121201(R) (2020).
- [22] K. Dolui, A. Suresh, and B. K. Nikolić, Spin pumping from antiferromagnetic insulator spin-orbit-proximitized by adjacent heavy metal: A first-principles Floquet-nonequilibrium Green function study, *arXiv:2109.15249* (2021).
- [23] Y. Liu, Z. Yuan, R. Wesselink, A. A. Starikov, and P. J. Kelly, Interface enhancement of Gilbert damping from first Principles, *Phys. Rev. Lett.* **113**, 207202 (2014).
- [24] K. Chen and S. Zhang, Spin pumping in the presence of spin-orbit coupling, *Phys. Rev. Lett.* **114**, 126602 (2015).
- [25] L. Arrachea and M. Moskalets, Relation between scattering-matrix and Keldysh formalisms for quantum transport driven by time-periodic fields, *Phys. Rev. B* **74**, 245322 (2006).
- [26] O. Shevtsov and X. Waintal, Numerical toolkit for electronic quantum transport at finite frequency, *Phys. Rev. B* **87**, 085304 (2013).
- [27] C. P. Schmid *et al.*, Tunable non-integer high-harmonic generation in a topological insulator, *Nature* **593**, 385 (2021).
- [28] H.-C. Lin, Sources, effects, and modelling of interharmonics, *Math Probl. Eng.* **2014**, 730362 (2014).
- [29] B. Gaury, J. Weston, M. Santin, M. Houzet, C. Groth, and X. Waintal, Numerical simulations of time-resolved quantum electronics, *Phys. Rep.* **534**, 1 (2014).
- [30] A. Manchon, H. C. Koo, J. Nitta, S. M. Frolov, and R. A. Duine, New perspectives for Rashba spin-orbit coupling, *Nat. Mater.* **14**, 871 (2015).
- [31] B. S. Popescu and A. Croy, Efficient auxiliary-mode approach for time-dependent nanoelectronics, *New J. Phys.* **18**, 093044 (2016).
- [32] B. K. Nikolić, L. P. Zârbo, and S. Souma, Imaging mesoscopic spin Hall fow: Spatial distribution of local spin currents and spin densities in and out of multiterminal spin-orbit coupled semiconductor nanostructures, *Phys. Rev. B* **73**, 075303 (2006).
- [33] R. L. Cooper and E. A. Uehling, Ferromagnetic resonance and spin diffusion in supermalloy, *Phys. Rev.* **164**, 662 (1967).
- [34] G. Stefanucci and R. van Leeuwen, *Nonequilibrium Many-Body Theory of Quantum Systems: A Modern Introduction* (Cambridge University Press, Cambridge, 2013).
- [35] T. Kloss, J. Weston, B. Gaury, B. Rossignol, C. Groth and X. Waintal, Tkquant: a software package for time-dependent quantum transport, *New J. Phys.* **23**, 023025 (2021).
- [36] K. Hattori, Spin pumping from finite-sized electron systems in ballistic and diffusive transport regimes, *Phys. Rev. B* **75**, 205302 (2007).
- [37] G. Tatara, Green's function representation of spin pumping effect, *Phys. Rev. B* **94**, 224412 (2016).
- [38] U. Bajpai and B. K. Nikolić, Spintronics meets nonadiabatic molecular dynamics: Geometric spin torque and damping on dynamical classical magnetic texture due to an electronic open quantum system, *Phys. Rev. Lett.* **125**, 187202 (2020).
- [39] M. G. Vavilov, V. Ambegaokar, and I. L. Aleiner, Charge pumping and photovoltaic effect in open quantum dots, *Phys. Rev. B* **63**, 195313 (2001).
- [40] L. E. F. Foa Torres, Mono-parametric quantum charge pumping: Interplay between spatial interference and photon-assisted tunneling, *Phys. Rev. B* **72**, 245339 (2005).
- [41] O. Ly and A. Manchon, Spin-orbit coupling induced ultra-high harmonic generation from magnetic dynamics, *arXiv:2104.04001* (2021).
- [42] M. Lysne, Y. Murakami, M. Schüler, and P. Werner, High-harmonic generation in spin-orbit coupled systems, *Phys. Rev. B* **102**, 081121(R) (2020).
- [43] S. Ghimire and D. A. Reis, High-harmonic generation from solids, *Nat. Phys.* **15**, 10 (2019).
- [44] Y. Bai, F. Fei, S. Wang, N. Li, X. Li, F. Song, R. Li, Z. Xu, and P. Liu, High-harmonic generation from topological surface states, *Nat. Phys.* **17**, 311 (2021).
- [45] T. N. Ikeda and M. Sato, High-harmonic generation by electric polarization, spin current, and magnetization, *Phys. Rev. B* **100**, 214424 (2019).
- [46] S. Takayoshi, Y. Murakami, and P. Werner, High-harmonic generation in quantum spin systems, *Phys. Rev. B* **99**, 184303 (2019).
- [47] J. M. Marmolejo-Tejada, P.-H. Chang, P. Lazić, S. Smidstrup, D. Stradi, K. Stokbro, and B. K. Nikolić, Proximity band structure and spin textures on both sides of topological-insulator/ferromagnetic-metal interface and their charge transport probes, *Nano Lett.* **17**, 5626 (2017).
- [48] K. Dolui and B. K. Nikolić, Spin-orbit-proximitized ferromagnetic metal by monolayer transition metal dichalcogenide: Atlas of spectral functions, spin textures and spin-orbit torques in Co/MoSe<sub>2</sub>, Co/WSe<sub>2</sub> and Co/TaSe<sub>2</sub> heterostructures, *Phys. Rev. Mater.* **4**, 104007 (2020).
- [49] K. Dolui, M. D. Petrović, K. Zollner, P. P. Plecháč, J. Fabian and B. K. Nikolić, Proximity spin-orbit torque on a two-dimensional magnet within van der Waals heterostructure: Current-driven antiferromagnet-to-ferromagnet reversible nonequilibrium phase transition in bilayer CrI<sub>3</sub>, *Nano Lett.* **20**, 2288 (2020).
- [50] M. Gibertini, M. Koperski, A. F. Morpurgo, and K. S. Novoselov, Magnetic 2D materials and heterostructures, *Nat. Nanotech.* **14**, 408 (2019).
- [51] T. Olsen, Theory and simulations of critical temperatures in CrI<sub>3</sub> and other 2D materials: easy-axis magnetic order and easy-plane Kosterlitz-Thouless transitions, *MRS Commun.* **9**, 1142 (2019).
- [52] T. Seifert *et al.*, Efficient metallic spintronic emitters of ultrabroadband terahertz radiation, *Nat. Photon.* **10**, 483 (2016).
- [53] H. Qiu *et al.*, Ultrafast spin current generated from an antiferromagnet, *Nat. Phys.* **17**, 388 (2021).